EURASIAN PHYSICAL TECHNICAL JOURNAL

2025, Volume 22, No. 2 (52)

https://doi.org/10.31489/2025N2/109-120

Received: 20/01/2025 Revised: 24/05/2025 Accepted: 23/06/2025 Published online: 30/06/2025

Research Article

UDC 53.043

INVESTIGATION OF THE STRESS-STRAIN STATE DURING NEW COMBINED DEFORMATION TECHNOLOGY

Volokitina I.E.*, Panin E.A., Volokitin A.V., Fedorova, T.D., Latypova, M.A., Makhmutov B.B.

Karaganda Industrial University, Temirtau, Kazakhstan
*Corresponding author: irinka.vav@mail.ru

Abstract. *This paper presents the results of finite element modeling of a novel technology of combined deformation by radial-shear broaching and traditional drawing. Using DEFORM program, the parameters of stress-strain state and deformation forces were studied. A range of models with varying initial diameters of the workpiece, single and total compressions, and different temperatures of heating the workpiece were considered. It was revealed that the optimal conditions occurred at 30-25-20 scheme at a temperature of 900°C. However, this scheme can be recommended when the strength of the deforming equipment is sufficient. In other cases, it is necessary to select a scheme that allows for deformation without exceeding the limiting loads.*

Keywords: drawing, modelling, bar, steel, stress-strain state.

1. Introduction

The manufacture of high-quality carbon steel bars is a complex undertaking requiring a synthesis of traditional and contemporary metalworking methodologies. Conventional techniques, with their proven track record and years of application, ensure stability and predictability of outcomes. Nevertheless, their capacity to attain the highest quality and dimensional accuracy is constrained. Furthermore, these methods frequently incur substantial production costs, often due to considerable energy consumption and protracted processing cycles. Furthermore, traditional methods such as hot rolling frequently result in heterogeneity of the metal structure and an increased level of internal stresses, which have a detrimental effect on the properties of the finished product. For instance, during the rolling process, significant fluctuations in thickness and geometric parameters occur, necessitating subsequent additional processing, which increases the cost.

However, modern technologies, particularly those involving severe plastic deformation (SPD) [1-5] and progressive deformation methods such as radial-shear rolling (RSR) or hydrostatic extrusion, offer novel solutions to this challenge. Nevertheless, it should be noted that these modern methods also have their limitations, including the high cost of equipment and the complexity of mastering the technology, which can render them economically unprofitable for some enterprises [6-8].

The optimal approach to be adopted is the creation of flexible, modular technological processes that combine the advantages of both traditional and modern methods [9-11]. This approach enables the adaptation of the production process to the specific requirements of the customer, the utilization of the most effective methods at each stage of production, and the minimization of costs. It is imperative to acknowledge the role of heat treatment, a critical component in the production of carbon steel bars, in significantly extending the duration of the technological cycle and escalating costs. Consequently, it is imperative to minimize the number and duration of thermal operations. Optimal process design, therefore, entails the use of pressure treatment methods in a more efficient manner, thereby reducing the necessity for additional heat treatment.

For instance, the selection of the most appropriate deformation mode and tool can result in the attainment of the desired mechanical properties without the necessity for additional annealing or quenching.

The proposed innovative technology for deforming carbon steel rods is based on a combination of radial-shear broaching (RSB) and traditional drawing [12, 13]. The fundamental distinction between the two methodologies lies in the cessation of the roll drive during the RSB process. This configuration is designed to prevent the conflict between the two deformation methods that would otherwise be impossible to avoid in a traditional configuration. The cessation of drive during the RSB phase facilitates a seamless transition to the drawing phase, thereby enabling the effective integration of the merits of both methodologies. RSB ensures rough processing and preforming of the rod, while drawing ensures high dimensional accuracy and excellent surface quality. This technological integration enables the optimization of energy consumption, enhancement of productivity, and reduction of production costs, while ensuring the manufacture of bars that exhibit superior mechanical characteristics and exceptional surface quality.

The complexity of the processes involved in designing and optimizing plastic deformation using a complex loading scheme necessitates the implementation of multiscale analysis and numerical modelling support. A plethora of models of plasticizing stresses are employed in computer modelling. Some of these models are based on empirical equations, such as the Sabbat model, while others are based on physical principles and phenomena occurring in a deformable material. The DEFORM software package is utilized for the analysis of diverse metalworking and heat treatment processes. With the help of DEFORM it is possible:

- To test the developed process not experimentally, in real production, but virtually on a computer;
- To conduct a numerical experiment and, based on its results, make changes to the parameters of the technological process;
- To predict the nature of metal shaping during pressure treatment. This significantly reduces the cost of experimental research;
- To study the processes of metal deformation during different types of tool movement. It is possible to vary the friction conditions, the models of the medium and the rheological properties of the material;
- To evaluate the process for defects (formation of cracks, creases, non-filling of the stamp, etc.). The results include a force graph, stress, strain, and temperature distribution fields.

The utilization of modelling in DEFORM has been demonstrated to facilitate a reduction in the production time of structures and components, enhance their quality, and mitigate costs that may emerge during the production process.

The novelty of this work lies in the study of the stress-strain state of a carbon steel bar deformed by a novel combined technology in the DEFORM program. The key feature of this work is a comprehensive study of energy-force parameters at the theoretical level using FEM modeling. The data obtained will form the basis at the design stage of the experimental installation, which will avoid possible equipment breakdowns from overloads.

2. Materials and Methods

In order to analyze the stress-strain state in the DEFORM program, a number of models of the radial-shear broaching process with subsequent drawing were constructed. In these models, both geometric and technological parameters were varied with the objective of determining the most optimal process conditions. Geometric parameters, such as the initial diameter of the workpiece and the absolute compression at each of the two passes, were varied. Among the technological parameters, the initial temperature of the workpiece was varied. As a result, the following models were built:

- the workpiece with a diameter of 30 mm was compressed sequentially to 27 mm, then to 23 mm.;
- the workpiece with a diameter of 30 mm was compressed successively to 25 mm, then to 20 mm.;
- the workpiece with a diameter of 20 mm was compressed successively to 18 mm, then to 16 mm.

Each of these models was considered at three temperatures: 20°C, 500 °C and 900°C.

The material of the blank was steel 10. The following friction coefficients were set: at the contact of the workpiece with the rolls of the RSR mill – 0.4; at the contact of the workpiece with the fiber – 0.1. The rolls of the RSP mill were disconnected from the drive and rotated from friction upon contact with the workpiece. The compression in the rolls and in the fiber were set to be similar, i.e., for example, in the model 30-27-23, on the first pass, the gap between the rolls and the diameter of the drawing die were equal to 27 mm.

The mesh of finite elements on the workpiece was constructed using tetragonal elements. Their distribution on the workpiece was carried out according to two distribution criteria:

- using the Size Ratio coefficient equal to 6, which grinds the volume of elements in the loaded zones by 6 times compared to the rest of the zones;

- using two zones of local condensation of elements – "Mesh Window" with a coefficient of 0.1, located in two deformation zones – in the rolls and in the drawing tool. These windows additionally thicken the mesh by a factor of 10.

All this led to the fact that in both deformation zones, the average face length of the final element was 0.18 mm approximately.

3. Results and discussion

In the course of the study of the strain state, the parameter "equivalent strain" was considered, which is a cumulative parameter reflecting the accumulation of all types of deformation. As illustrated in Fig. 1, a comprehensive overview of the equivalent strain of all models is provided. As the results for all nine models are presented on a single scale of ε = 0-4, it can be observed that the strain patterns in the horizontal direction are consistent across all models.

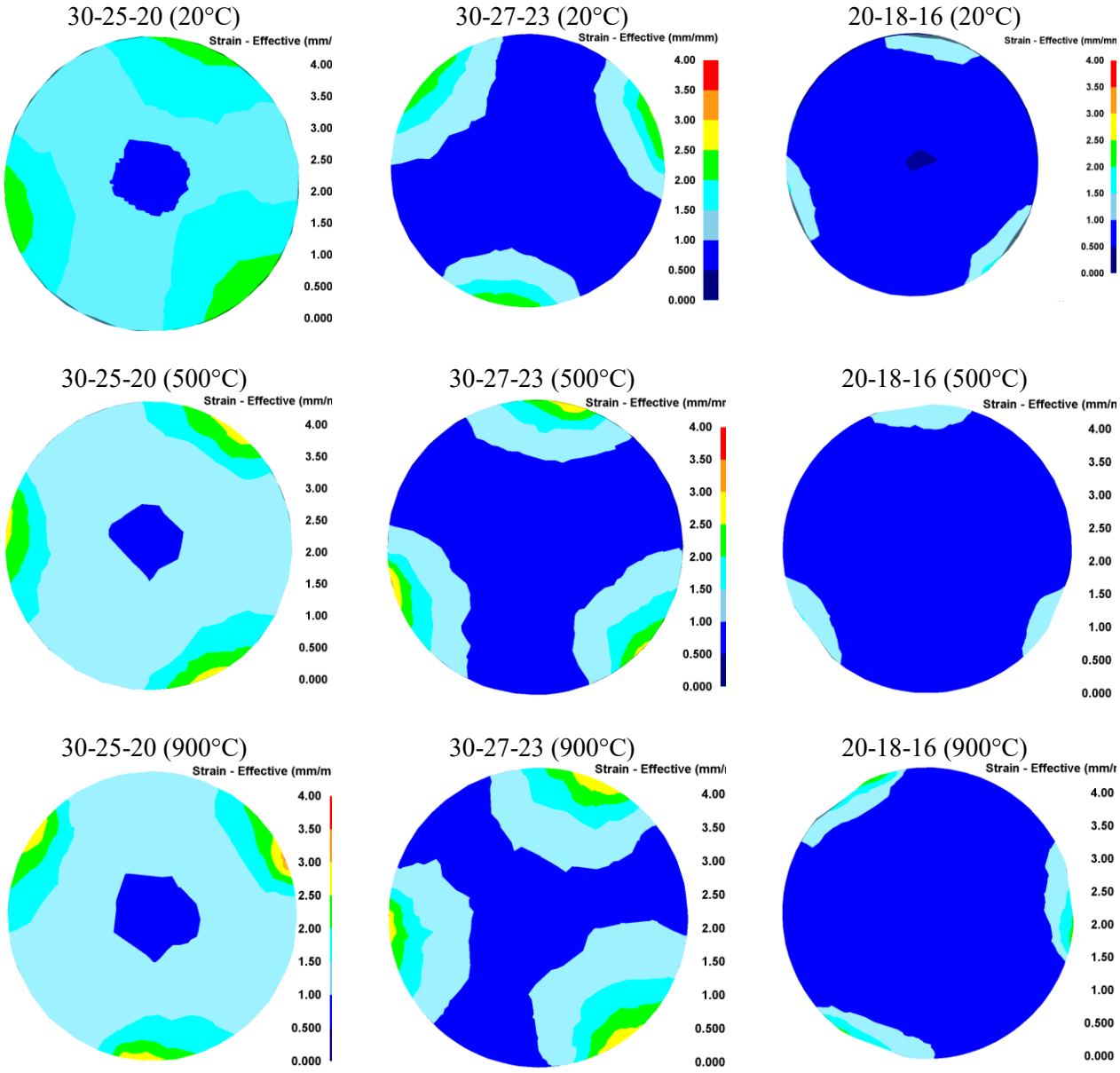

Fig. 1. Distribution of equivalent strain over the workpiece section

Furthermore, it is evident that models 30-25-20 exhibit the maximum metal processing over the entire cross-section at all temperatures considered. This phenomenon can be attributed to the highest values of single compression and total compression (10 mm versus 7 mm and 4 mm). A comparable outcome was achieved in a study of conventional zirconium RSR [14]. In the 30-27-23 model, the processing effect is slightly lower, but it is still at a fairly high level in the areas of contact with the rolling rolls. The lowest effect is observed in models 20-18-16. In this model, the level of processing in the surface layers is comparable to the level of elaboration of the central zone in model 30-25-20.

It is evident from the presented patterns of vertical strain that the initial temperature of the workpiece exerts a significant influence on the distribution of strain, both in terms of its extent and its nature. In this instance, the predominant effect of elevated strain is discernible solely in the surface areas of the workpiece. In areas of direct contact with rolling rolls, an increase in temperature leads to an enhancement in the metal's malleability, resulting in a gradual increase in strain. To quantify the strain state, the obtained values of equivalent strain in the surface zones and in the center were summarized in the resulting diagram in Fig. 2.

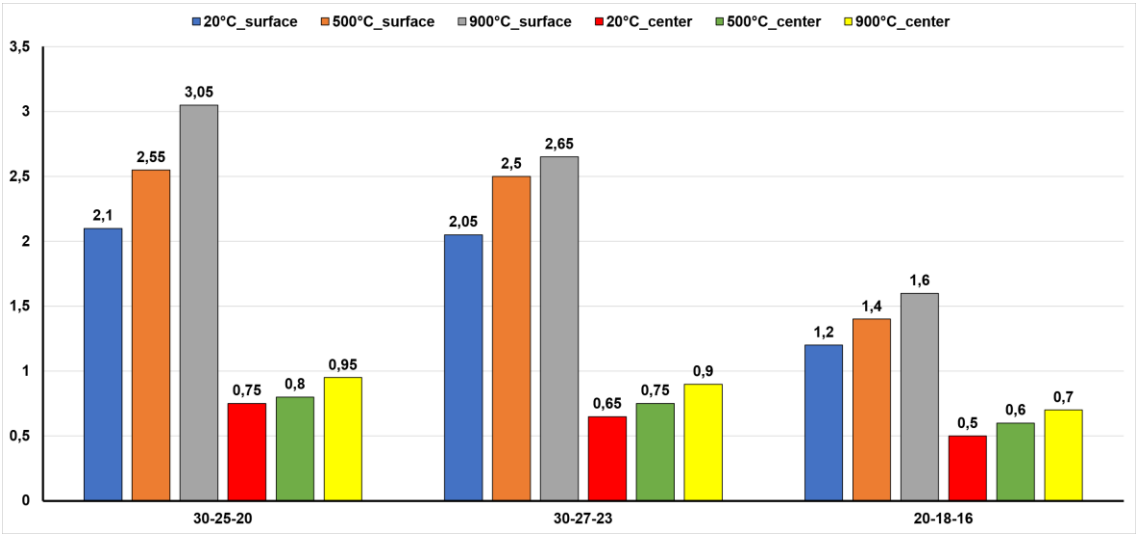

Fig. 2. Numerical values of equivalent strain

As illustrated in the diagram, the maximum strain values exceeding 3 are observed at maximum compression in the 30-25-20 model at an elevated temperature of 900°C. Concurrently, a decline in temperature to ambient levels results in a reduction in the degree of processing in the surface areas by approximately 25-30% across all models. Furthermore, a comparison of the values at constant temperatures reveals a heightened sensitivity to the degree of compression. To illustrate this point, we may consider the strain level in model 30-25-20 as the baseline. A decrease in the total compression level by 3 mm (model 30-27-23) results in a 15% decrease in deformation at 900°C. However, this difference diminishes to 3% as the temperature is reduced, thereby reducing the ductility of the metal in the areas of contact with the rolls. A further decrease in the total compression level by 3 mm (model 20-18-16) results in a 48% difference in strain values at 900°C, while with a decrease in temperature, this difference decreases to 42%. Consequently, it can be deduced that the extent of equivalent strain in the process under investigation is more dependent on the total compression applied. While the influence of temperature is also observed, its effect is significantly less pronounced.

It is evident that analogous dependencies of the strain amount on the total compression and temperature are sustained for the central layers of the workpiece. However, the location of the rolling rolls in the space in the form of a RSR mill leads to the fact that at the broaching stage, strain develops only in the surface zones, and the central region receives an increase in strain only at the drawing stages. Consequently, an uneven gradient structure emerges in the cross-section of the workpiece, exhibiting a disparity in equivalent strain ranging from 200% to 300%. It is also noteworthy that the central zone of the workpiece demonstrates minimal processing across all cases, with strain levels ranging from $\varepsilon = 0.5 - 0.7$ at room temperature, and reaching $\varepsilon = 0.7 - 0.95$ at elevated temperatures of 900°C.

In order to study the stress state, there are a number of recommended parameters that must be selected, with the consideration of the strain pattern being of particular importance. For instance, within the ECAP

process, the study of the equivalent stress is adequate due to the utilization of an all-encompassing compression scheme. In the studied combined process of radial-shear broaching with drawing, there are both compression zones from the action of deforming tools and stretching zones from the action of a pulling force applied to the front end of the workpiece. Consequently, the most appropriate approach would be to analyze the average hydrostatic pressure, which accounts for the direction of the applied stresses. As illustrated in Fig. 3, the images depict the average hydrostatic pressure within the workpiece section situated within the deformation zone of the rolling rolls. A comparison of the obtained patterns of average hydrostatic pressure as a function of total compression (in the horizontal direction) reveals a direct proportional relationship.

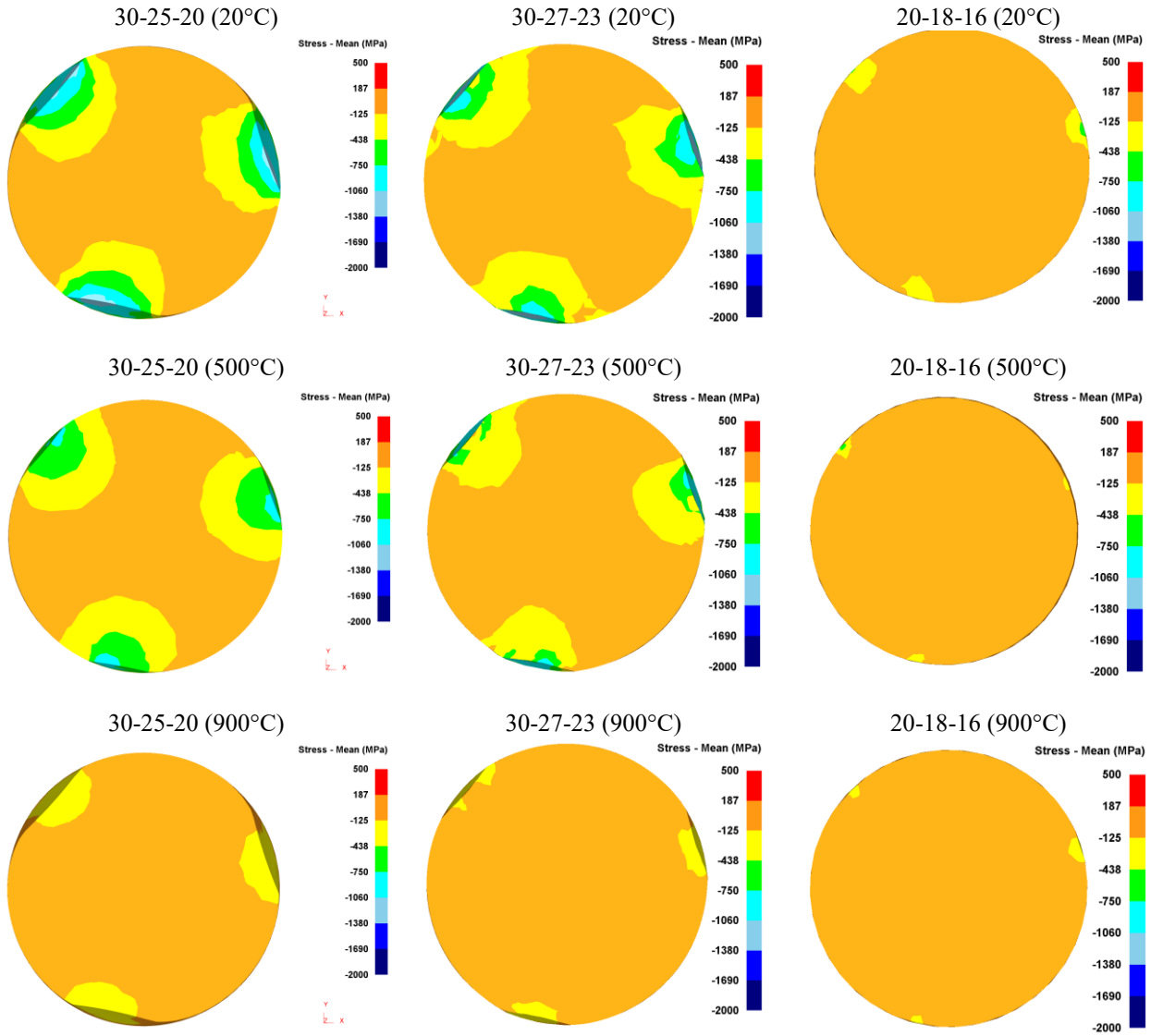

Fig. 3. Distribution of the average hydrostatic pressure over the workpiece cross section in the deformation zone of the rolling rolls

The highest levels of compressive stresses are observed in models 30-25-20, where the compression value is maximum. With a decrease in total compression, compressive stresses decrease, and a decrease in the length of direct impressions from contact with the rolls is also clearly visible. In addition, an inverse proportional relationship is evident when comparing the patterns of average hydrostatic pressure as a function of temperature (in the vertical direction). The highest level of compressive stresses is observed in models where the workpiece temperature is 20°C. As the temperature increases, the level of compressive stresses decreases, as well as the extent of the deformation zones. In order to quantify the stress state, the values of the average hydrostatic pressure on the surface and in the deformation zone of the rolling rolls were summarized in the resulting diagram in Fig. 4.

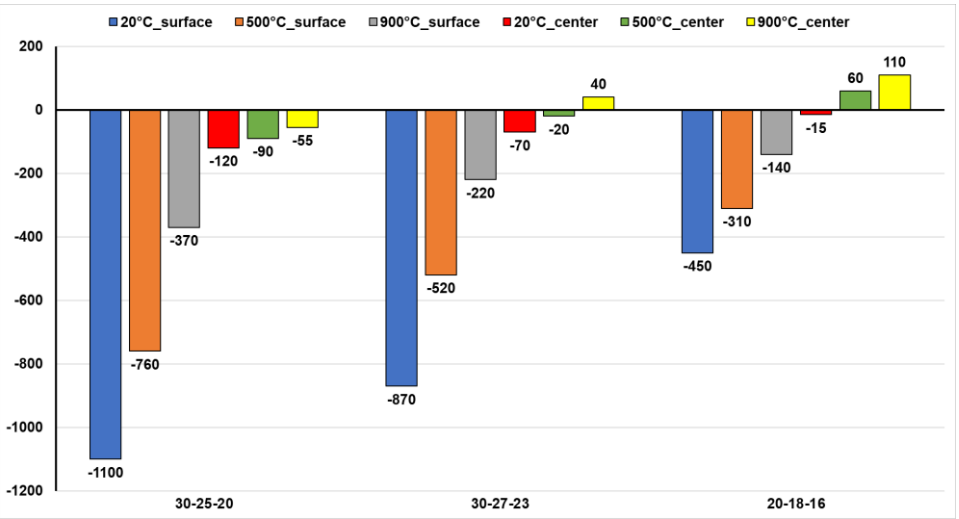

Fig. 4. Numerical values of the average hydrostatic pressure in the deformation zone of rolling rolls

As illustrated in the diagram, the maximum values of the average hydrostatic pressure above 1 GPa are attained at maximum compression in the 30-25-20 model at a temperature of 20°C. An increase in temperature to 900°C leads to a decrease in the level of average hydrostatic pressure in the surface zones by approximately threefold. A parallel comparison of the values at constant temperatures reveals a high degree of correlation with the extent of compression. For instance, when the total compression level is reduced by 3 mm (model 30-27-23), the pressure level decreases by approximately 20% at 20°C. However, as the temperature rises, this difference increases to 40%, resulting in enhanced ductility of the metal in the areas of contact with the rolls. A further decrease in the total compression level by 3 mm (model 20-18-16) results in an increase in the strain values at 20°C of almost 60%, with an increase in temperature causing an enhancement of this difference to 65%.

In considering the pressure within the central layers of the workpiece, it is important to note their comparatively low level in relation to the surface layers. Concurrently, under certain conditions (at an elevated temperature of 900°C), tensile stresses reaching up to 100 MPa begin to act within this zone. This heterogeneous stress state gives rise to a gradient of properties across the workpiece cross-section. Consequently, it can be deduced that the mean hydrostatic pressure during the process under scrutiny is found to be considerably influenced by both the total compression and the temperature of the workpiece.

In the analysis of deformation forces, the force values on each passage for each deforming tool (rolls and lugs) were taken into consideration. The resultant force graphs for the 30-25-20 model are presented in Fig. 5. The graphs for rolls are shown in red, and for drawing dies in green. A close examination of the graphs reveals that the most significant exertions take place during the drawing stages. Concurrently, the level of effort exerted during the initial pass invariably surpasses that of the subsequent pass, which is concomitant with a diminution in the length of the deformation zone within the drawing die. This reduction in length is attributable to a general decrease in the workpiece diameter. The influence of the heating temperature on the nature of the graphs is also clearly noticeable. At a temperature of 20°C, all graphs exhibit an even horizontal appearance. However, when the workpiece is heated to 500°C during the initial stage of radial-shear broaching, the graph exhibits an upward trend, indicating the workpiece's cooling and a reduction in the ductility of the material. Conversely, at the subsequent stage (the initial stage of drawing), the temperature has already decreased to a sufficient extent, resulting in the force graph acquiring a horizontal appearance. However, when the workpiece is heated to 900°C, the force graphs at the first stage of radial shear broaching, the first stage of drawing, and the second stage of radial-shear broaching have an increasing appearance, indicating a prolonged cooling process for the workpiece.

A quantitative analysis of the forces reveals that the maximum level of 209 kN is attained at the initial stage of drawing in the model at 20°C, with a subsequent decline to 130 kN at the subsequent stage. With an increase in temperature to 500°C, a force of approximately 182 kN is observed at the first stage of drawing, and at the second stage of drawing, the force is around 112 kN. When the workpiece is heated to 900°C at the first stage of drawing, a force of about 170 kN is exerted at the end of the stage, and at the second stage of drawing, the force is about 124 kN.

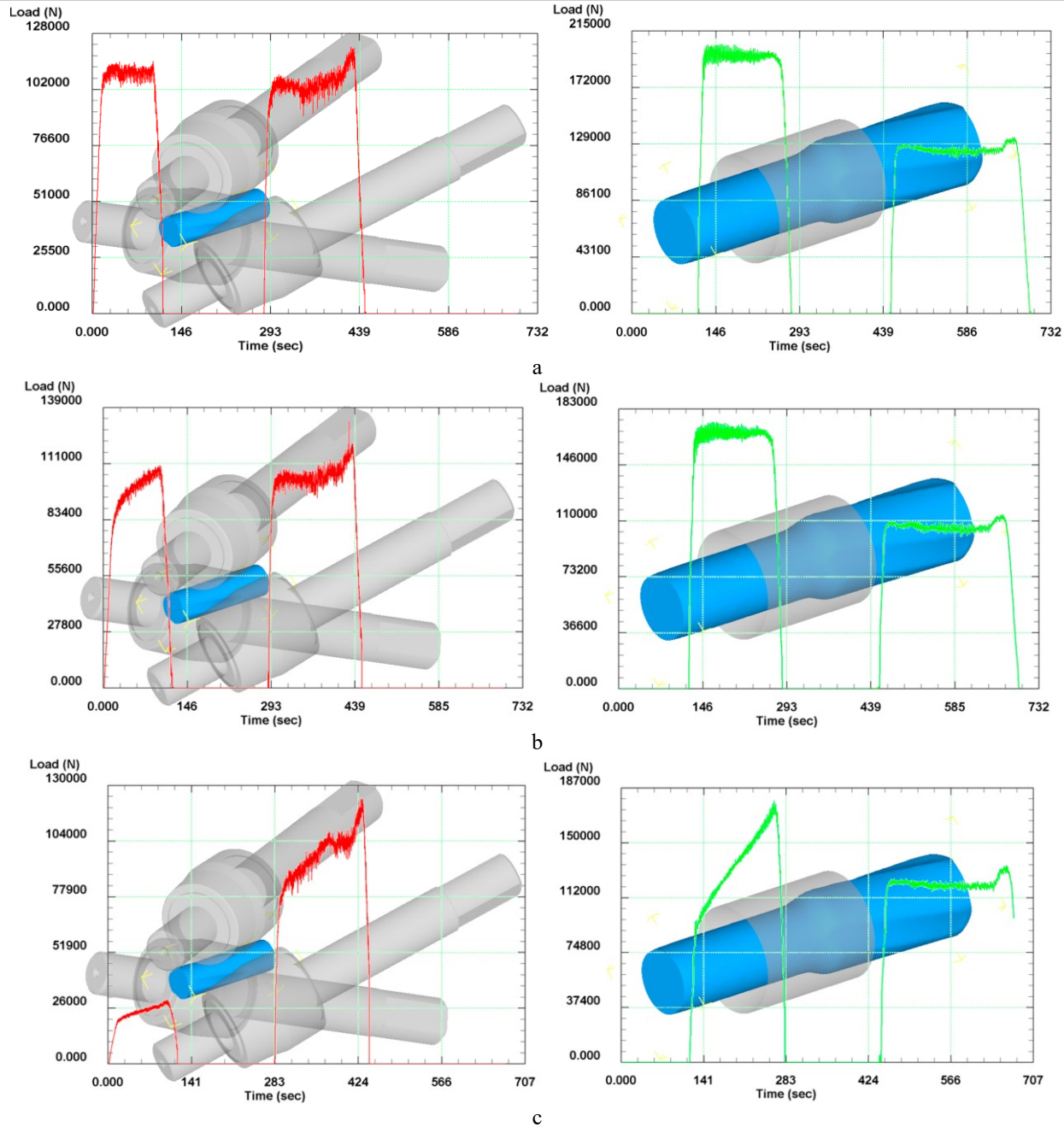

Fig. 5. Force graphs for the 30-25-20 model: a – at 20°C; b - at 500°C; c - at 900°C

Notwithstanding the elevated heating temperature, a greater degree of force was documented at the second stage of the drawing process. The underlying reason for this phenomenon becomes evident when analyzing the force graphs of radial shear stretching. At 20°C, the initial stage of radial shear broaching yielded a force of 108 kN, while the subsequent stage resulted in an approximate force of 117 kN. It is noteworthy that the force graphs at both stages exhibited a horizontal trajectory, indicating the absence of a cooling factor for the workpiece. At 500°C, the graph at the first stage of radial shear broaching has an inclined appearance due to the reduction in ductility of the material resulting from the cooling of the workpiece, with a force of 108 kN being reached at the end of the stage. At the second stage of radial shear broaching, the force is approximately 117 kN, and the force graph at this stage has a horizontal appearance. At 900°C in the initial stage of radial shear broaching, the force reduces to 28 kN by the conclusion of the stage. Concurrently, the augmentation in exertion at this stage is less pronounced in comparison to the preceding instance, signifying a diminished cooling intensity of the more heated workpiece. In the

subsequent stage of radial shear broaching, the force curve exhibits an upward trend, reaching a maximum of 105 kN before leveling off, suggesting the termination of the pronounced cooling process. Subsequently, a force jump of up to 128 kN, a hallmark of the RSR scheme, occurs, denoting the output of the workpiece from the rolls [14]. Fig.6 shows the force graphs for the 30-27-23 model.

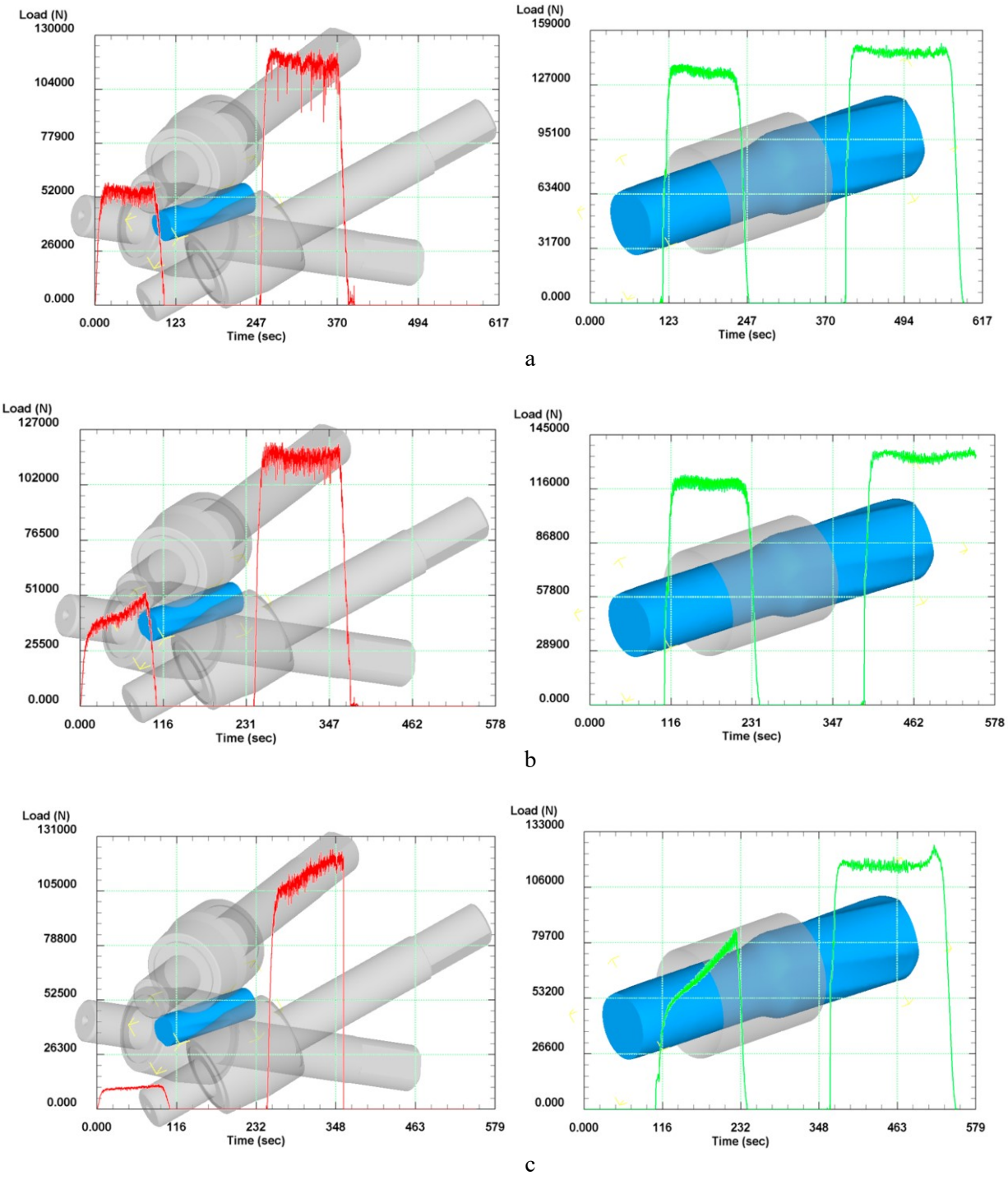

Fig. 6. Force graphs for the 30-27-23 model: a – at 20°C; b - at 500°C; c - at 900°C

In this model, it is necessary to take into account the unevenness of the compression: in the initial stages, the compression is 3 mm, whereas in the subsequent stages, it is 4 mm. Consequently, the drawing forces of the second stage at all temperatures exceed the drawing forces of the first stage. This phenomenon

is also the underlying cause of the increased force difference observed during the stages of radial shear broaching. As observed in the 30-25-20 model, the maximum effort is also encountered during the drawing stages. At 20°C, a force of 130 kN is generated during the initial stage of drawing, while the subsequent stage generates approximately 150 kN. The force graphs at both stages exhibit a horizontal trajectory, owing to the absence of cooling of the workpiece. Drawing graphs at a temperature of 500°C demonstrate a similar appearance, with the cooling process concluding at the initial stage of radial shear broaching. At 500°C, the graphs for the first stage of drawing show a force of 118 kN, and for the second stage, the force is approximately 140 kN. At 900°C, the nature of the graphs is similar to the previously considered 30-25-20 model – at the first stage of drawing, the graph has an oblique appearance, as the workpiece cools intensively, which ends at the second stage of radial shear broaching. The second stage of drawing is distinguished by the absence of cooling, resulting in a horizontal graph. At 900°C, a force of 80 kN is generated during the initial stage of drawing, while at the subsequent stage, the force increases to approximately 128 kN.

In the initial phase of radial-shear broaching at 20°C, a force of 53 kN is generated. At the subsequent stage, the force increases to approximately 125 kN. The force graph at both stages exhibits a horizontal trajectory. At 500°C, the graph at the first stage of radial shear broaching has an inclined appearance, reaching 50 kN at the end of the stage. At the second stage of radial shear broaching, the force is approximately 120 kN, and the force graph at this stage has a horizontal appearance. At 900°C in the initial stage of radial shear broaching, the force reaches a mere 10.5 kN at the conclusion of the stage. Concurrently, the augmentation in force at this stage is found to be negligible, in contrast to the 30-25-20 model, which can be attributed to a diminution in the cooling intensity due to a reduction in the value of a single compression from 5 mm to 3 mm. The force graph of the second stage of radial shear broaching also exhibits an upward trend, which becomes horizontal at approximately 120 kN, suggesting the termination of the intensive cooling process. The absence of a force jump in this model can be attributed to the disparity in single and total compression of the same workpiece with a diameter of 30 mm.

As demonstrated in Fig. 7, the force graphs for the 20-18-16 model are presented. In contradistinction to the preceding model (30-27-23), it is imperative to consider the uniformity of compression in this model. At both stages, the uniformity of compression is 2 mm; however, the diameter of the initial blank is reduced to 20 mm. Consequently, a decrease in the length of the deformation focus is observed at all deformation zones, resulting in a substantial reduction in effort when compared to blank models with a diameter of 30 mm. Notably, this model exhibits an opposite effect, where maximum forces are attained at all temperatures during the second stage of radial-shear broaching. Concurrently, the magnitude of the force at the initial stage of radial-shear broaching is found to be negligible, with a maximum recorded force of 6.5 kN.

At 20°C, a force of 64 kN is generated during the initial stage of drawing, while at the subsequent stage, the force reduces to approximately 50 kN. The force graphs for both stages exhibit a horizontal trajectory, a consequence of the inadequate cooling of the workpiece. Drawing graphs at a temperature of 500°C demonstrate a similar appearance – here, cooling ceases at the initial stage of radial shear broaching. At 500°C, a force of 56 kN is generated during the initial stage of drawing, and in the subsequent stage, the force is approximately 42 kN. At 900°C, the nature of the graphs is similar to that of the previously considered models 30-25-20 and 30-27-23. At the first stage of drawing, the graph has an oblique appearance due to intensive cooling of the workpiece. Conversely, the second stage of drawing is distinguished by the absence of cooling, resulting in a horizontal graph. At 900°C, a force of 46 kN is generated during the initial stage of drawing, while at the subsequent stage, the force reduces to approximately 40 kN.

At the initial stage of radial-shear broaching at 20°C, a force of 6.5 kN is generated, while at the subsequent stage, the force increases to approximately 62 kN. Notably, the force graphs at both stages exhibit a horizontal orientation. At 500°C, the graph at the first stage of radial shear broaching has an inclined appearance, reaching 5 kN at the end of the stage. At the second stage of radial shear broaching, the force is approximately 55 kN, and the force graph at this stage has a horizontal appearance. At 900°C, the force at the end of the first stage of radial shear broaching is only 1.5 kN. In the subsequent stage of radial shear broaching, the force increases to approximately 47 kN. It is evident that the absence of a force jump in this model is attributable to the reduced diameter of the initial workpiece.

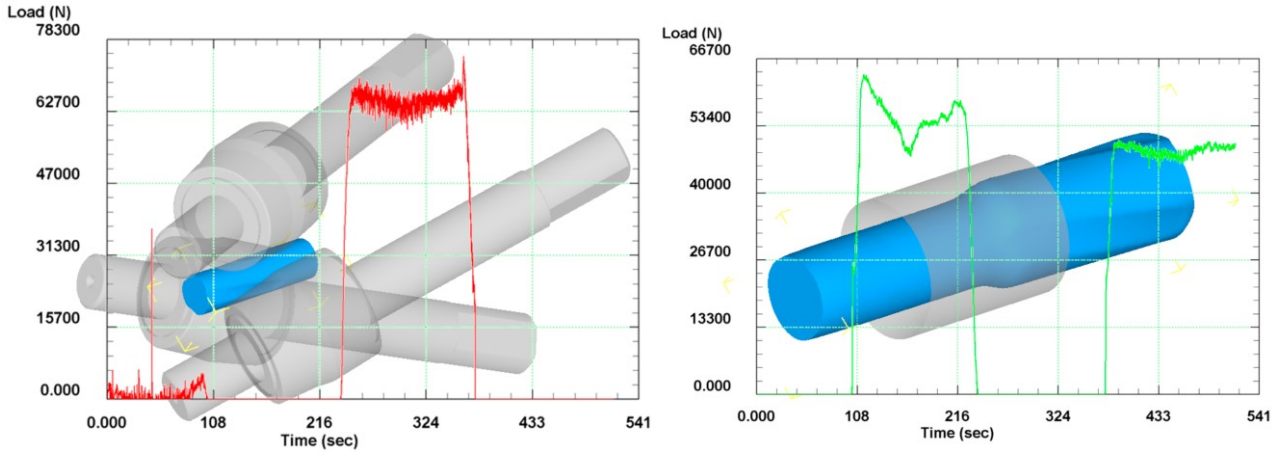

a)

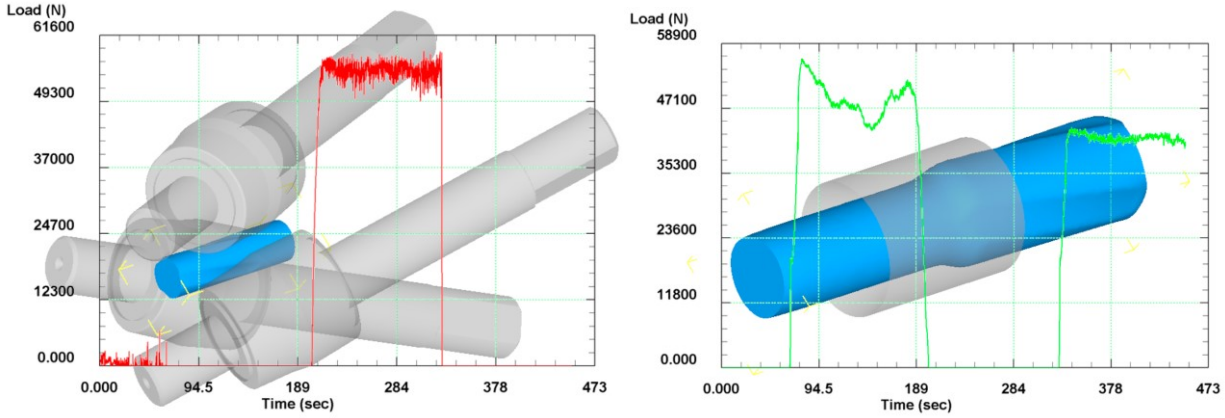

b)

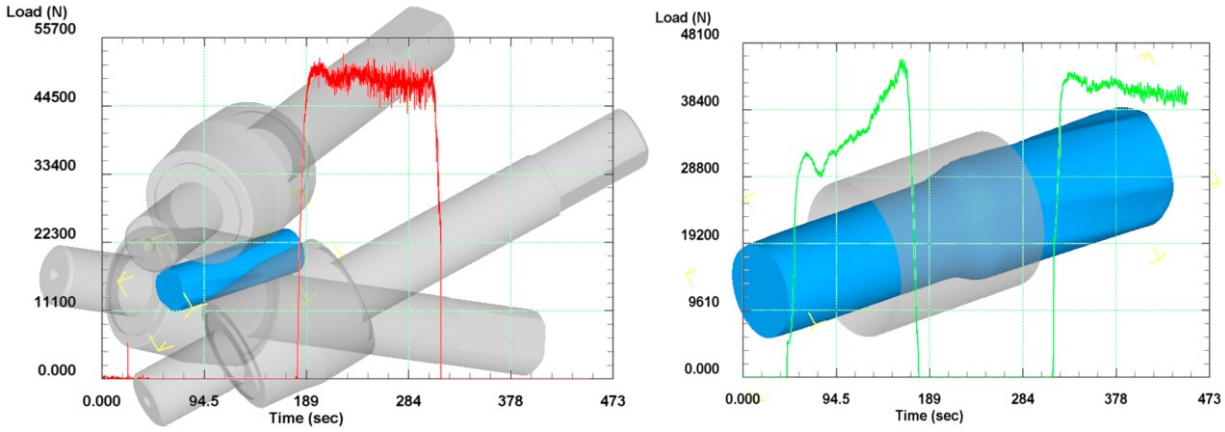

c)

Fig. 7. Force graphs for the 20-18-16 model: a – at 20°C; b - at 500°C; c - at 900°C

4. Conclusion

The paper employed finite element modelling of the radial-shear broaching process, followed by drawing in the Deform program, to study the stress-strain state and energy-strength parameters. A range of models with varying initial diameters of the workpiece, single and total compressions, and different temperatures of heating the workpiece were considered. The study revealed that the optimal processing of the metal occurred under the 30-25-20 scheme at a temperature of 900°C, with the 30-27-23 scheme demonstrating comparable efficacy. Concurrently, it is imperative to acknowledge the substantial reduction in compressive stresses that occurs at elevated temperatures. The selection of the deformation scheme is

paramount, and the values of the deformation forces must be given due consideration, as they provide a comprehensive representation of the loads occurring at all stages of the process. It is noteworthy that a considerable degree of effort is required for models with a blank of 30 mm. However, when the strength of the deforming equipment is sufficient, the 30-25-20 scheme can be recommended. In cases where this is not the case, it is necessary to select a scheme that allows for deformation without exceeding the limiting loads.

Conflict of interest statement

The authors declare that they have no conflict of interest in relation to this research, whether financial, personal, authorship or otherwise, that could affect the research and its results presented in this paper.

CRediT author statement

Conceptualization, I.V.; Methodology, E.P. and A.V.; Software, A.V.; Validation, T.F., M.L and I.V.; Formal Analysis, I.V. and A.V.; Investigation, E.P. and B.M.; Resources, B.M.; Data Curation, I.V. and M.L.; Writing – Original Draft Preparation, I.V. and E.P; Writing – Review & Editing, I.V.; Visualization, E.P.; Supervision, A.V. and M.L. The final manuscript was read and approved by all authors.

Funding

This research has been/was/is funded by the Science Committee of the Ministry of Science and Higher Education of the Republic of Kazakhstan (Grant No. AP19678974).

References

1 Surzhikov A.P., Lysenko E.N., Malyshev A.V., Petrova A., Ghyngazov S.A., Aimukhanov A.K. (2020) Phase transformations in ferrites during radiation-thermal sintering. *Eurasian phys. tech. j.*, 17, 1, 144-153. https://doi.org/10.31489/2020No1/26-34

2 Nurumgaliyev A., Zhuniskaliyev T., Shevko V., Yerekeyeva G. (2024) Modeling and development of technology for smelting a complex alloy (ligature) Fe-Si-Mn-Al from manganese-containing briquettes and high-ash coals. *Scientific Reports*, 14, 1, 7456. https://doi.org/10.1038/s41598-024-57529-6

3 Issagulov A.Z., Kim V.A. Kvon S.S., Kulikov V.Y., Tussupova A.U. (2014) Production of technical silicon and silicon carbide from rice-husk. *Metalurgija*, 53(4), 685–688. Available at: https://hrcak.srce.hr/122222

4 Sapargaliyeva B., Agabekova A., Syrlybekkyzy S., Kolesnikov A., Ulyeva G., Yerzhanov A., Kozlov P. (2023) Study of changes in microstructure and metal interface Cu/Al during bimetallic construction wire straining. *Case Studies in Construction Materials*, 18, e02162. https://doi.org/10.1016/j.cscm.2023.e02162

5 Kovalev P.V., Popova S.D., Issagulov A.Z., Kulikov V.Y., Kvon S.S. (2017) Investigation of the effect of high strength strips steel modification with rare-earth metal (REM). *Metalurgija*, 56(3-4), 393–395. Available at: https://hrcak.srce.hr/180992

6 Naseri R. (2017) An experimental investigation of casing effect on mechanical properties of billet in ECAP process. *Intern. Journal of Advanced Manufacturing Technology*, 90, 3203–3216. https://doi.org/10.1007/s00170-016-9658-1

7 Denissova A., Kuatbay Y., Liseitsev Y. (2023) Effect of thermomechanical processing of building stainless wire to increase its durability. *Case Studies in Construction Materials*, 19, e02346. https://doi.org/10.1016/j.cscm.2023.e02346

8 Kawasaki M., Ahn B., Lee H.J., Zhilyaev A.P., Langdon T.G. (2015) Using high-pressure torsion to process an aluminum–magnesium nanocomposite through diffusion bonding. *J. Mater. Res.*, 31, 88-99. https://doi.org/10.1557/jmr.2015.257

9 Panichkin A., Wieleba W. Kenzhegulov A., Uskenbayeva A.M, Kvyatkovskii S., Kasenova B. (2023) Effect of thermal treatment of chromium iron melts on the structure and properties of castings. *Materials Research Express*, 10(8), 086502. https://doi.org/10.1088/2053-1591/acead7

10 Albert M., Schilling K. (2015) The line coating robot – An automated mobile system for high precision powder coating. *Proceeding of the 2nd IFAC Conference on Embedded Systems. Computer Intelligence and Telematics*, 28, 10, 58-62. https://doi.org/10.1016/j.ifacol.2015.08.108

11 Volokitin A.V., Panin E.A., Latypova M.A., Kassymov S.S. (2022) Microstructure evolution of steel-aluminum wire during deformation by "equal-channel angular pressing-drawing" method. *Eurasian phys. tech. j.*, 19, 1, 73-77. https://doi.org/10.31489/2022No1/73-77

12 Volokitina I., Volokitin A., Makhmutov B. (2024) Formation of Symmetric Gradient Microstructure in Carbon Steel Bars. *Symmetry*, 16(8), 997. https://doi.org/10.3390/sym16080997

13 Volokitina I., Volokitin A., Panin E. (2024) Gradient microstructure formation in carbon steel bars. *Journal of Materials Research and Technology*, 31, 2985–2993. https://doi.org/10.1016/j.jmrt.2024.07.038

14 Arbuz A., Kawalek A., Ozhmegov K., Dyja H., Panin E., Lepsibayev A., Sultanbekov S., Shamenova R. (2020) Using of Radial-Shear Rolling to Improve the Structure and Radiation Resistance of Zirconium-Based Alloys. *Materials*, 13, 19, 4306. https://doi.org/10.3390/ma13194306

AUTHORS' INFORMATION

Volokitina, Irina Evgenievna – PhD, Professor, Department of Metallurgy and Materials Science, Karaganda Industrial University, Temirtau, Kazakhstan; Scopus Author ID: 55902810800, ORCID: 0000-0002-2190-5672; irinka.vav@mail.ru

Panin, Evgeny Alexandrovich – PhD, Professor, Department of Metal forming, Karaganda Industrial University, Temirtau, Kazakhstan; Scopus Author ID: 55903153300, ORCID: 0000-0001-6830-0630; cooper802@mail.ru

Volokitin, Andrei Valeryevich – PhD, Associate Professor, Department of Metal forming, Karaganda Industrial University, Temirtau, Kazakhstan; Scopus Author ID: 56524247500, ORCID: 0000-0002-0886-3578; dyusha.vav@mail.ru

Fedorova, Tatiana Dmitrievna – Master, Department of Metallurgy and Materials Science, Karaganda Industrial University, Temirtau, Kazakhstan; Scopus Author ID: 57222628232; ORCID: 0009-0005-6117-1297, tanyusik88@bk.ru

Latypova, Marina Alexandrovna – Master, Accounting and audit, Karaganda Industrial University, Temirtau, Kazakhstan, Scopus Author ID: 57219097120, ORCID: 0000-0003-4340-6134; marinapray@mail.ru

Makhmutov, Bolat Bizhanovich – Candidat of Technical Sciences, Vice-Rector for Research and International Co-operation, Karaganda Industrial University, Temirtau, Kazakhstan; Scopus Author ID: 57356852600, ORCID: 0009-0001-8978-8097; bb.makhmut@tttu.edu.kz